Title

25-Hydroxycholesterol Protects Host against Zika Virus Infection and Its Associated Microcephaly in a Mouse Model

Journal

Immunity, 46(3)

ISSN

1074-7613

Authors

Li, Chunfeng
Deng, Yong-Qiang
Wang, Shuo
et al.

Publication Date

2017-03-01

DOI

10.1016/j.immuni.2017.02.012

Peer reviewed

HHS Public Access

Author manuscript

Immunity. Author manuscript; available in PMC 2018 May 17.

Published in final edited form as:

Immunity. 2017 March 21; 46(3): 446–456. doi:10.1016/j.immuni.2017.02.012.

25-Hydroxycholesterol Protects Host against Zika Virus Infection and Its Associated Microcephaly in a Mouse Model

Chunfeng Li[1,2,11], **Yong-Qiang Deng**[2,11], **Shuo Wang**[3,11], **Feng Ma**[1,4,11], **Roghiyh Aliyari**[4,11], **Xing-Yao Huang**[2,11], **Na-Na Zhang**[2,5], **Momoko Watanabe**[6], **Hao-Long Dong**[2], **Ping Liu**[7], **Xiao-Feng Li**[2], **Qing Ye**[2], **Min Tian**[2,8], **Shuai Hong**[3], **Junwan Fan**[3], **Hui Zhao**[2], **Lili Li**[7], **Neda Vishlaghi**[6], **Jessie E. Buth**[6], **Connie Au**[4], **Ying Liu**[7], **Ning Lu**[7], **Peishuang Du**[7], **F. Xiao-Feng Qin**[1], **Bo Zhang**[9], **Danyang Gong**[10], **Xinghong Dai**[10], **Ren Sun**[10], **Bennett G. Novitch**[6,*], **Zhiheng Xu**[3,*], **Cheng-Feng Qin**[2,5,*], and **Genhong Cheng**[1,4,12,*]

[1]Center for Systems Medicine, Institute of Basic Medical Sciences, Chinese Academy of Medical Sciences & Peking Union Medical College, 100005 Beijing, China; Suzhou Institute of Systems Medicine, Suzhou, 215123 Jiangsu, China

[2]Department of Virology, State Key Laboratory of Pathogen and Biosecurity, Beijing Institute of Microbiology and Epidemiology, 100071 Beijing, China

[3]State Key Laboratory of Molecular Developmental Biology, CAS Center for Excellence in Brain Science and Intelligence Technology, Institute of Genetics and Developmental Biology, Chinese Academy of Sciences; Parkinson's Disease Center, Beijing Institute for Brain Disorders, 100101 Beijing, China

[4]Department of Microbiology, Immunology and Molecular Genetics, University of California, Los Angeles, CA 90095, USA

[5]Guangxi Medical University, 530021 Nanning, China

[6]Department of Neurobiology and Eli & Edythe Broad Center of Regenerative Medicine and Stem Cell Research, University of California, Los Angeles, CA 90095, USA

[7]CAS Key Laboratory of Infection and Immunity, Institute of Biophysics, Chinese Academy of Sciences, Chaoyang District, 100101 Beijing, China

[8]Beijing Traditional Medicine Chinese Hospital, Capital Medical University, 100069 Beijing, China

[*]Correspondence: bnovitch@ucla.edu (B.G.N.), zhxu@genetics.ac.cn (Z.X.), qincf@bmi.ac.cn (C.-F.Q.), gcheng@mednet.ucla.edu (G.C.).

[11]Co-first author

[12]Lead Contact

SUPPLEMENTAL INFORMATION

Supplemental Information includes Supplemental Experimental Procedures and seven figures and can be found with this article online at http://dx.doi.org/10.1016/j.immuni.2017.02.012.

AUTHOR CONTRIBUTIONS

G.C., C.-F.Q., Z.X., and B.G.N. jointly directed the research. C.L., Y.-Q.D., and S.W. designed and performed most of the experiments. C.L. and F.M. wrote most of the manuscript. R.A. helped with writing and editing the manuscript, performing the organoids-based experiments and liposome-binding assay. X.-Y.H., C.L., and H.-L.D. performed monkey experiments. N.-N.Z, M.W., P.L., X.-F.L., Q.Y., M.T., S.H., J.F., H.Z., L.L., N.V., J.E.B., C.A., Y.L., N.L., P.D., F.X.-F.Q., B.Z., D.G., X.D., and R.S. helped to perform experiments or contribute to reagents. Everyone contributed to the writing.

[9]CAS Key Laboratory of Special Pathogens and Biosafety, Center for Emerging Infectious Diseases, Wuhan Institute of Virology, Chinese Academy of Science, 430071 Wuhan, China

[10]Department of Molecular and Medical Pharmacology and California NanoSystems Institute, University of California, Los Angeles, Los Angeles, CA 90095, USA

SUMMARY

Zika virus (ZIKV) has become a public health threat due to its global transmission and link to severe congenital disorders. The host immune responses to ZIKV infection have not been fully elucidated, and effective therapeutics are not currently available. Herein, we demonstrated that cholesterol-25-hydroxylase (CH25H) was induced in response to ZIKV infection and that its enzymatic product, 25-hydroxycholesterol (25HC), was a critical mediator of host protection against ZIKV. Synthetic 25HC addition inhibited ZIKV infection in vitro by blocking viral entry, and treatment with 25HC reduced viremia and conferred protection against ZIKV in mice and rhesus macaques. 25HC suppressed ZIKV infection and reduced tissue damage in human cortical organoids and the embryonic brain of the ZIKV-induced mouse microcephaly model. Our findings highlight the protective role of CH25H during ZIKV infection and the potential use of 25HC as a natural antiviral agent to combat ZIKV infection and prevent ZIKV-associated outcomes, such as microcephaly.

In Brief

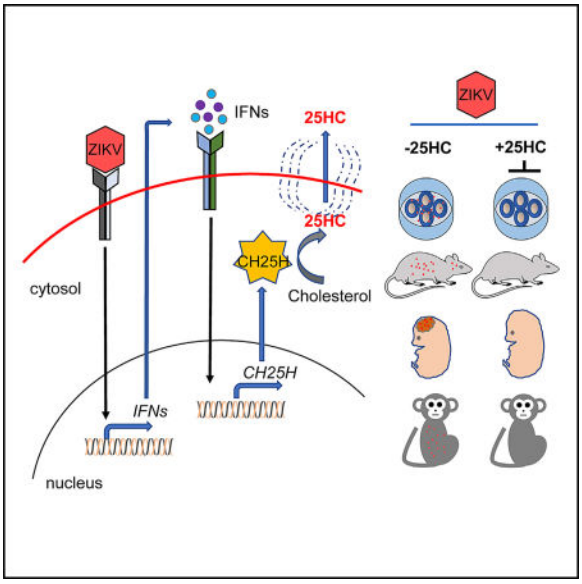

Zika virus (ZIKV) presents a major challenge to the global health system. Li et al. find that 25-hydroxycholesterol (25HC) inhibits ZIKV infection in monkeys and human cortical organoids and protects mice from microcephaly. 25HC has potential as a first-line antiviral agent to combat a broad array of pathogenic species, including ZIKV.

INTRODUCTION

Zika virus (ZIKV) is an increasing global health threat due to the rapidly expanding range of its mosquito vector, international travel of asymptomatic carriers, and the ability to be sexually transmitted (D'Ortenzio et al., 2016; Driggers et al., 2016; Musso and Gubler, 2016; Rasmussen et al., 2016). ZIKV was initially isolated from an infected sentinel rhesus monkey in the Zika forest of Ugandain 1947 (Dick et al., 1952). ZIKV infection only caused mild symptoms in past epidemics, such as arthralgia, malaise, rash, and conjunctivitis (Musso and Gubler, 2016). Its appearance in Brazil in 2015 was accompanied by unexpected outbreaks of congenital malformations such as microcephaly, Guillain-Barré syndrome (GBS), and meningoencephalitis (Cao-Lormeau et al., 2016; Carteaux et al., 2016). These severe neurological manifestations are now attributed to ZIKV, with intrauterine infection of pregnant women occasionally leading to microcephaly, spontaneous abortion, and intrauterine growth restriction due to placental insufficiency (Brasil et al., 2016; Miner et al., 2016). Moreover, ZIKV infection can lead to male infertility in mice through testicular damage (Ma et al., 2016). Therefore, ZIKV infection presents a huge challenge to the global health system.

ZIKV infects neural progenitor cells (NPCs) generated from human-induced pluripotent stem cells (hiPSCs) (Tang et al., 2016), resulting in cell death and inhibition of cell-cycle progression. The 3D-cultured organoid model recapitulates brain development at an early stage and provides an in vitro system to study the molecular mechanisms by which ZIKV infection of pregnant mothers results in neurological disorders in the fetus (Garcez et al., 2016; Qian et al., 2016). Three research groups, including ours, established the direct link between ZIKV infection and microcephaly in mice (Cugola et al., 2016; Li et al., 2016a; Miner et al., 2016). ZIKV infection in mouse NPCs results in cell apoptosis, cell-cycle arrest, and reduction of NPC differentiation, ultimately leading to cortical thinning and microcephaly (Li et al., 2016a).

Unfortunately, there is no approved antiviral drug or vaccine to combat ZIKV. The murine model of ZIKV pathogenesis is limited to the type I interferon (IFN) signaling knockout line (*Ifnar*$^{-/-}$), suggesting the potentially protective role of IFN-stimulated genes (ISGs) during ZIKV infection (Lazear et al., 2016). Further evidence comes from recent studies showing that the host controls ZIKV infection through IFN signaling pathways (Bayer et al., 2016), which protect cells from viral infection by inducing numerous ISGs (Sadler and Williams, 2008). Recently, interferon-induced transmembrane 1 and 3 proteins (IFITM1 and IFITM3) were demonstrated to inhibit ZIKV infection in early stages of the viral life cycle, and IFITM3 can prevent ZIKV-induced cell death (Savidis et al., 2016). However, the role of other ISGs in host immunity against ZIKV infection remains largely elusive.

Cholesterol-25-hydroxylase (CH25H) is an ISG that encodes an enzyme that oxidizes cholesterol to 25-hydroxycholesterol (25HC) (Holmes et al., 2011; Liu et al., 2012). 25HC is a natural oxysterol, which controls sterol biosynthesis by regulation of nuclear receptors and sterol-responsive element binding protein (SREBP) activity (Janowski et al., 1999). CH25H is also involved in the innate immune response to toll-like receptor (TLR) ligands and IFN (Bauman et al., 2009; Park and Scott, 2010). It has been shown that 25HC-mediated

induction of retinoic acid-inducible gene-I (RIG-I) in macrophages and the endothelium mediates atherosclerotic inflammation through induction of interleukin-8 (IL-8) (Brown and Jessup, 1999; Wang et al., 2012). We and others have recently revealed that CH25H and its product, 25HC, inhibit infection by a broad range of pathogenic viruses, including vesicular stomatitis virus (VSV), human immunodeficiency virus (HIV), and Ebola virus (EBOV) (Blanc et al., 2013; Liu et al., 2013), but the role of CH25H and 25HC during ZIKV infection remains unknown.

In the present study, we revealed the protective role of CH25H against ZIKV infection and characterized the protective effects of 25HC in combating ZIKV infection in human cells, brain organoids, fetal mice, and macaques.

RESULTS

ZIKV Infection Induces *CH25H* and Triggers CH25H-Dependent Antiviral Activity

We investigated the role of CH25H in anti-ZIKV immunity and evaluated its expression in a ZIKV-infected human alveolar epithelial cell line (A549) using RNA sequencing (RNA-seq). ZIKV infection upregulated (Log_2[fold change]>1) multiple well-characterized antiviral ISGs such as *MX1, ISG15, OASL, CH25H*, and other genes named ZIG (ZIKV-induced genes) (Figure 1A). Quantitative reverse transcription PCR (qRT-PCR) assays were performed to validate the RNA-seq results and confirmed that ZIKV infection led to the induction of *CH25H* in a dose-dependent manner (Figure 1B). ZIKV infection also significantly induced *IFNB* (Figure S1A), followed by dramatic induction of *CH25H* (Figure S1B), as well as other ISGs, such as *IP10, IFITM3, ISG15, MX1, STING*, and *RIG-I* (Figures S1C–S1H). Similarly, treating cells with recombinant IFN-β elevated the *CH25H* level in A549 cells (Figure S1I).

To further determine the role of CH25H during ZIKV infection, *CH25H* knockout A549 cells were generated using the CRISPR/Cas9 system (Figures S2A and S2B) and were subjected to ZIKV infection. Both qRT-PCR and plaque assays (Figures 1C and 1D) demonstrated that CH25H deficiency significantly enhanced ZIKV replication in A549 cells compared to wild-type (WT) cells. Furthermore, overexpression of CH25H in HeLa cells significantly inhibited ZIKV replication, similar to the inhibitory impact of IRF1, which was used as a positive control (Figure 1E). However, overexpression of CH25H-M, which carries a mutation in the active site of the enzyme (hydroxylase activity-dead mutant) (Chen et al., 2014), showed no significant effect on ZIKV infection (Figure 1E), suggesting that the enzymatic activity of CH25H is essential for its antiviral function. HeLa cells were transfected with plasmids expressing CH25H and CH25H-M, and after 24 hr, the supernatants were used to treat baby hamster kidney-21 (BHK-21) cells. The supernatants from HeLa cells overexpressing CH25H, but not CH25H-M, significantly inhibited ZIKV infection in BHK-21 cells (Figure 1F) and HeLa cells (Figure S3A). Furthermore, the presence of 25HC in the media from WT CH25H-overexpressing cells was confirmed by mass spectrometry (MS) analysis (Figures S3B and S3C).

Together, these results indicated that CH25H is induced in response to ZIKV infection in mammalian cells and may play a protective role against ZIKV infection through its enzymatic product, 25HC.

25HC Broadly Inhibits Flavivirus Infection by Blocking Viral Entry

One of the major barriers in antiviral therapy is potential cytotoxicity. Therefore, we investigated the cytotoxicity of 25HC using Vero (African green monkey kidney) cells. We found that 25HC at concentrations as high as 10 μM showed no obvious cytotoxicity (Figure S4A). However, cells were protected from ZIKV at a concentration of 0.4 μM of 25HC, as measured by plaque assay (Figures 2A and S4B). These results were also confirmed by qRT-PCR and immunofluorescence assays (Figures 2B, S4C, and S4D). The IC_{50} of 25HC against ZIKV was calculated to be 188 nM (Figure 2C), which was similar to that of the well-characterized pan-flavivirus polymerase inhibitor NITD008 (Deng et al., 2016; Yin et al., 2009). We further tested the antiviral efficacy of 25HC against other flavivirus members, including Dengue virus (DENV), yellow fever virus (YFV), and West Nile virus (WNV), and found that the IC_{50}s of 25HC were 406, 526, and 1109 nM, respectively (Figures 2D–2F). These results demonstrated that 25HC is a potent pan-flavivirus inhibitor.

To determine which step of the flavivirus life cycle is inhibited by 25HC, ZIKV genomic RNA from the supernatant of the infected cells treated with 25HC were measured by qRT-PCR. 25HC blocked ZIKV replication in both 25HC, pre- or post-treated cells (Figure S5A). However, the inhibitory effect of 25HC observed in post-treated cells was less than the effect in pre-treated cells (Figure S5A). Next, a cell-binding assay was conducted in Vero cells. The results showed that viral binding to the host was not affected by 25HC treatment (Figure S5B), indicating that 25HC does not affect the cell-binding capability of ZIKV. An internalization assay was performed in BHK-21 cells as previously described (Talarico et al., 2005). 25HC blocked ZIKV internalization in a dose-dependent manner, while NITD008, an adenosine nucleoside inhibitor that inhibits the RdRp (RNA-dependent RNA polymerase) activity of DENV (Yin et al., 2009), failed to do so (Figure 3A). In addition, a syncytia formation assay in C6/36 cells was done to investigate whether 25HC inhibits flavivirus-mediated cell-to-cell fusion (Zaitseva et al., 2010). Similar to the 4G2 monoclonal antibody —a flavivirus envelope protein antibody—used as a positive control, 25HC prevented DENV2-mediated cell-to-cell fusion in mosquito cells (Figure 3B and Figure S5C). We were able to show that the addition of an artificial liposome that can merge with the A549 cell membrane was able to compete with 25HC for membrane incorporation and reduced the anti-ZIKV function of 25HC in a dose-dependent manner (Figure 3C). ZIKV and DENV replicon assays showed that 25HC did not inhibit ZIKV or DENV RNA replication (Figure 3D) when compared to NITD008. 25HC was able to inhibit ZIKV infection in *IFNAR1*$^{-/-}$ A549 cells (Figure S5D), indicating that the inhibitory function of 25HC to ZIKV infection was independent of the type I IFN signaling pathway. Therefore, unlike NITD008, 25HC inhibited flavivirus infection by blocking its entry at the early stage of infection.

25HC Reduces ZIKV Viremia and Improves Survival in Mice

As our in vitro data indicated that 25HC promoted anti-viral activity against ZIKV, we next tested the in vivo antiviral effects of 25HC in 3- to 4-week-old immunocompetent BALB/c

mice as described previously (Larocca et al., 2016; Zhang et al., 2016). Animals were treated with 25HC (50 mg/kg) or vehicle and infected with ZIKV strain GZ01/2016 intraperitoneally (i.p.). ZIKV RNA in serum was measured one day post-infection (dpi) by qRT-PCR. 25HC treatment significantly reduced viremia in mice compared to the vehicle (Figure 4A).

Furthermore, we evaluated the in vivo antiviral activity of 25HC in the IFN-α/β-receptor-deficient A129 mouse model (Lazear et al., 2016). ZIKV-inoculated A129 mice treated with the vehicle died within 14 dpi (Figure 4B) with severe neurological symptoms, including hind limb weakness and paralysis. Treatment with 50 mg/kg of 25HC reduced mortality significantly (Figure 4B), and the surviving mice developed no clinical symptoms. Viremia measured at 4 and 7 dpi was considerably reduced in 25HC-treated mice (Figures 4C and 4D). The ZIKV titer in the brains of 25HC-treated animals was also reduced at 7 dpi (Figure 4E). These results suggested that 25HC efficiently protects mice from ZIKV-associated morbidity and mortality.

25HC Protects Rhesus Monkeys from ZIKV Infection

We further evaluated the protective effect of 25HC against ZIKV infection in the nonhuman primate (NHP) model (Dudley et al., 2016). Five animals were challenged with 10^3 PFU of ZIKV, of which two were treated with 25HC (1.5 mg/kg/day, intravenously [i.v.]) and three were used as control. At this dose, robust viremia (duration 2–4 days) and detectable uremia were seen in the untreated group (Figures 5A and 5B). In contrast, ZIKV was undetectable in both the urine and serum of the 25HC-treated group (Figures 5A and 5B). These results suggest that 25HC significantly inhibited ZIKV infection in NHPs.

To further evaluate the therapeutic impact of 25HC in the NHP model (Li et al., 2016b), we challenged four rhesus monkeys with a higher dose of 10^5 PFU ZIKV. Two of the animals received 25HC, one prior to ZIKV challenge and one post-ZIKV challenge. At this higher dose, the two untreated control NHPs experienced fever (axillary temperature > 38.9°C), while body temperature was not significantly increased in animals that received 25HC (Figure S6A). ZIKV RNA was readily detected in the serum and urine in both control animals. 25HC pretreatment 24 hr before challenge shortened the duration of viremia and viral shedding in the urine (Figures S6B and S6C). 25HC treatment 4 hr post-challenge also shortened ZIKV RNA shedding in the urine (Figure S6C). Together, these results suggested that 25HC can attenuate ZIKV infection and prevent fever in monkeys.

Viral infection triggers strong innate immune responses, including the release of inflammatory cytokines that, when overexpressed (Iwasaki and Pillai, 2014; Osuna et al., 2016), can be harmful to the host (Bayless et al., 2016). ZIKV (10^5 PFU) infection induced the expression of IFN-γ, IL-15, and CXCL9 cytokines, and Luminex assay results showed that 25HC treatment reduced their production in NHP serum (Figure 5C). Our results indicated that 25HC treatment reduces ZIKV infection and its induced symptoms in NHPs.

25HC Inhibits ZIKV Infection in Human Cortical Organoids

To investigate whether 25HC can protect against ZIKV-associated neurological damage, we tested its effects in the human cortical organoids (HCO) differentiated from embryonic stem

cells. HCOs grown in three-dimensional culture (3D culture) were infected with ZIKV strain PRVABC59/2015 after 23 days of development in vitro. ZIKV replicated efficiently in the HCOs as measured by qRT-PCR (Figure 6A). ZIKV infection also triggered induction of *IFNB* (Figure 6B) and *CH25H* (Figure 6C) 12, 48, and 72 hr post-infection. Pretreatment with as little as 0.5 μM of 25HC significantly suppressed ZIKV infection in the organoids, and 2.5 μM treatment resulted in 90% reduction of ZIKV genomic RNA (Figure 6D). Pretreatment overnight with 25HC at a concentration of 2.5 μM significantly protected HCOs from ZIKV infection as measured by plaque assay (Figure 6E). These results were also confirmed by immunofluorescence assay, where the 2.5 μM 25HC treatment almost completely protected brain organoids from ZIKV infection (Figure 6F). These results together demonstrated that 25HC can effectively protect developing human cortical tissue from ZIKV infection.

25HC Inhibits ZIKV Infection in the Embryonic Mouse Brain and Protects against ZIKV-Induced Microcephaly

It has been reported that ZIKV efficiently replicates in the brains of fetal mice and causes microcephaly (Li et al., 2016a). We have shown here that 25HC protects mice from ZIKV-induced viremia and death and infection of human cortical tissue in vitro. Therefore, we investigated whether 25HC could protect the embryonic mouse brain from ZIKV infection and resultant microcephaly.

We infected or mock-infected littermate brains at embryonic day 13.5 (E13.5) and inspected them at E18.5. Pregnant mice were treated daily with 25HC or vehicle (HβCD). The number of infected cells in the cerebral cortex was significantly reduced in 25HC-treated animals compared to the vehicle-treated group (Figure 7A). ZIKV RNA levels in brain tissues were also dramatically decreased by 25HC (Figure 7B). We further investigated whether 25HC treatment of pregnant mice could prevent ZIKV-associated fetal microcephaly. ZIKV infection led to a significant reduction in brain size, enlarged lateral ventricles, and a thinner marginal zone (MZ), cortical plate (CP), and ventricular zone/subventricular zone (VZ/SVZ) (Figures 7C and 7D). The incidence of these developmental defects was significantly reduced upon 25HC treatment of ZIKV-infected pregnant mice (Figures 7C and 7D). It was notable that the sub-plate was lost in the ZIKV-infected cortex, yet detectable in 25HC-treated mice (Figures 7D and 7E). We also stained the cortex at E18.5 with different neuronal markers, including Tbr1 and NeuN. We found that ZIKV infection led to a thinner cortex and decreased the density of $NeuN^+$ neurons, particularly in the outer layers, and these phenotypes could be partially rescued by 25HC treatment (Figure 7E).

Cell-cycle deregulation of neuronal progenitor cells (NPCs) and cell death are critical factors in microcephaly development (Li et al., 2016a). Therefore, we investigated the effects of 25HC on cell proliferation and cell death in ZIKV-infected fetal mouse brains. As shown in Figure 7F, ZIKV infection considerably reduced the population of phosph-H3 positive cells (P-H3, a marker for NPC in the M phase), and 25HC treatment rescued this phenotype. In addition, ZIKV infection of the fetal brains led to massive cell death, as shown by the number of cells positive for the activated form of caspase 3, which was significantly reduced by 25HC treatment (Figure 7G).

Our studies demonstrated no cytotoxic effects from administering up to 10 μM of 25HC to Vero cells in vitro (Figure S4A). Pregnant mice pretreated with 50 mg/kg of 25HC from E14.5 for five days showed no significant weight changes or adverse effects on their pregnancy (Figure S7A). The birth and condition (growth and weight) of neonatal mice were also not affected by 25HC (Figures S7A and S7B). A129 mice injected i.p. with 25HC for seven days showed no changes in ALT levels (Figure S7C). Furthermore, the bioavailability of 25HC in the serum of BALB/c mice pretreated with 25HC by i.p. route was tested. The serum concentration of 25HC peaked at 1 μM at approximately 4 hr post-injection and returned to normal levels 24 hr post-injection (Figure S7D).

The above results demonstrated that 25HC treatment of pregnant mice not only prevents ZIKV infection in the fetal brain, but also significantly reduces the incidence of microcephaly.

DISCUSSION

A major goal of antiviral drug development is to discover drugs that are not only effective against known targets, but also have potential applications against unforeseen outbreaks of new emerging infections, such as ZIKV. The innate immune system uses effector molecules that are naturally very broadly acting; therefore, one promising antiviral strategy is to find ways to stimulate those molecules.

Type I IFNs and their downstream ISGs combat a large variety of pathogens and play a critical role in host defense against ZIKV, as *Ifnar*$^{-/-}$ mice do not survive infection (Lazear et al., 2016). However, the contributions of individual ISGs in protecting the host from ZIKV remain unclear. Our current study shows that a specific ISG, *CH25H*, is induced in host cells and human brain organoids during ZIKV infection. We have also demonstrated that CH25H plays a critical role in host defense against ZIKV, as overexpression of CH25H strongly suppresses the infection in multiple cell types, and *CH25H*$^{-/-}$ A549 cells are more susceptible to ZIKV infection. Previous studies, including ours, have indicated that CH25H conducts its antiviral activities through the production of small antiviral molecule 25HC, which is dependent on its hydroxylation activity (Blanc et al., 2013; Liu et al., 2013). However, we have also shown that CH25H inhibits hepatitis C virus through direct interaction with NS5A, which is a hydroxylase-independent mechanism (Chen et al., 2014).

We have compared the antiviral activities of WT and mutated CH25H and demonstrated that the mutation abolishing the hydroxylase activity also diminished the antiviral activity against ZIKV, suggesting the essential role of the CH25H enzymatic activity in ZIKV inhibition. Using the well-established viral internalization assay, DENV-mediated cell-to-cell fusion model, and liposome-binding assay, we provided further evidence that 25HC did not affect ZIKV-host cell binding, but rather inhibited viral entry. These results are consistent with our previous observations that 25HC inhibits viral entry by suppressing fusion between viral and cell membranes in VSV, HIV, and Nipah virus infections (Liu et al., 2013). Our results showed that 25HC could inhibit ZIKV infection in type I IFN signaling deficient A549 cells and in *Ifnar*$^{-/-}$ mice. However, 25HC may suppress ZIKV infection through other immune pathways, like activating integrated stress response (ISR) genes (Shibata et al., 2013) or the

TLR4-dependent NF-kB pathway as described (Aye et al., 2012), which needs to be further investigated.

Recently, Zmurko et al. (2016) have found that 7-deaza-2′-Cmethyla-denosine (7DMA), a nucleotide analog known to suppress DENV infection by blocking viral RNA synthesis, inhibited ZIKV replication in vitro and in the AG129 mouse model. However, its activity was not potent enough to resolve ZIKV infection, and it had cytotoxic effects. Xu et al. (2016) screened ~6,000 molecules, including drugs that were approved or under investigational use, to discover which of them could inhibit ZIKV replication in neural cells. They found that several compounds, including emricasan, niclosamide, and inhibitors of cyclin-dependent kinases, could inhibit ZIKV replication or disrupt infection-induced caspase-3 activity. Although the impact of these molecules on ZIKV infection in vivo has not been investigated, Barrows et al. found that more than 20 out of ~700 FDA-approved drugs screened had inhibitory effects on ZIKV infection in vitro (Barrows et al., 2016; Xu et al., 2016), yet their in vivo effects also remain to be inspected. Our previous results showed that naturally produced 25HC has the potential to be a broad antiviral agent by demonstrating its ability to not only suppress HIV and MHV68 infection in vitro and in vivo, but also inhibit other highly pathogenic viruses such as EBOV, RVFV, and Nipah virus in vitro (Liu et al., 2013).

In this study, we have taken comprehensive approaches, in multiple in vitro and in vivo models, to illustrate the efficacy of 25HC against ZIKV infection and its associated microcephaly. We showed that 25HC inhibits infection by ZIKV and other flaviviruses, including DENV, YFV, and WNV. Treatment with 25HC pre- or post-ZIKV infection significantly reduces the morbidity and mortality in mice and considerably reduces fever and viremia in monkeys. We have identified a compound that protects against ZIKV-related congenital microcephaly in mice. 25HC is an endogenous oxysterol, which can penetrate the cell membrane and the blood-brain barrier (Woollett, 2001). This is consistent with our results showing that i.p. administration of 25HC in pregnant mice rescues ZIKV-related microcephaly. 25HC is a natural anti-viral molecule produced by the host during cholesterol metabolism. Moreover, it was found that oxysterols like 24HC, 25HC, and 27HC inhibited HIV replication in vitro (Moog et al., 1998). It will be intriguing to investigate the effects of other oxysterols against ZIKV infection in the future. However, it has previously been reported that 25HC could have toxic effects on placental trophoblasts in vitro at a high dose (30 μM) (Larkin et al., 2014). This finding should be investigated more carefully in the future before using 25HC in pregnant women.

In conclusion, our study presents a ZIKV inhibitor that not only reduces viremia in mice and monkeys, but also protects infected fetal mice from microcephaly. Since 25HC is a natural product of lipid metabolism and can modify host membranes to block viral entry, it has great potential as a first-line antiviral agent to combat a broad array of viruses, including emerging and pathogenic species such as ZIKV.

EXPERIMENTAL PROCEDURES

Mice, Monkey, and Ethics Statements

129/Sv/Ev mice deficient in IFN-α/β receptors (A129 mice) were kindly provided by Qi-Bin Leng (Institut Pasteur of Shanghai, Chinese Academy of Sciences). BALB/c mice were purchased from Jackson Laboratory. All mice were bred in our animal facility. Rhesus monkeys (*Macaca mulatta*) were purchased from the Laboratory Animal Center, Academy of Military Medical Science. All experimental procedures involving animals were performed according to protocols approved by the Animal Experiment Committee of Laboratory Animal Center, Academy of Military Medical Sciences (IACUC-13-2016-001).

Virus, Cells, and Reagents

ZIKV strains (GZ01/2016, GenBank: KU820898; SZ01/2016, GenBank: KU866423; and FSS13025/2010, GenBank: JN860885), DENV2-43, YFV-17D, and WNV-chin01 used in this study. A549, BHK-21, HeLa, and Vero cells were purchased from ATCC and cultured in DMEM media (37°C, 5% CO2). C6/36 cells were cultured in RPMI1640 medium (28°C, 5% CO2). All media were supplemented with 10% FBS (ExCell Bio, Jiangsu), 100 units/mL penicillin, and 50 μg/mL streptomycin. The hybridoma D1-4G2-4-15 (ATCC: HB-112) was used to produce antibody 4G2. Plasmids expressing GFP, IRF1, and CH25H were from GeneCopoeia and described in our previous study (Liu et al., 2013). CH25H hydroxylase activity-dead mutant (CH25H-M) was mutated from a WT CH25H construct as described previously (Chen et al., 2014). 25-Hydroxycholesterol (25HC) and (2-Hydroxypropyl)-β-cyclodextrin (HβCD) were purchased from Sigma. NITD008 was a kind gift from Pei-Yong Shi (Novartis Institute for Infectious Diseases).

Plaque Assay

BHK-21 cells were seeded in a 12-well plate for 12 hr. Cells were washed with 1 × PBS once and infected with the viruses used in this study for 1 hr. Viral inoculations were aspirated and replaced with DMEM containing 1% low-melting agarose and 2% FBS. Viral plaques were developed at 4 dpi.

ZIKV Internalization Assay

BHK-21 cells in 12-well plate were pretreated with 25HC for 12 hr followed by infection with ZIKV (200 PFU) at 4°C for 1 hr. After 1 hr, cells were washed with cold 1 × PBS three times to remove the un-bound viruses, followed by incubating cells at 37°C for 1 hr to allow for virus internalization. Cells were washed once by 1 × PBS and treated with 0.2 mL of citric acid buffer (citric acid 40 mM, potassium chloride 10 mM, sodium chloride 135 mM, pH 3.0) for 1 min to inactivate bound, but not internalized, viruses as described (Talarico et al., 2005). Plaque assay was performed with the BHK-21 cells immediately. The PFU numbers in EtOH-treated samples were set to 100%.

ZIKV Infection in Mice

3- to 4-week-old female BALB/c orA129 mice were treated with 25HC (50 mg/kg) or the HβCD vehicle intraperitoneally (i.p.) 12 hr prior to infection i.p. with ZIKV strain

GZ01/2016. The treatment was continued daily for seven days. Mice were observed daily for signs of illness or morbidity until 21 dpi. The survival rate was evaluated using the Log-rank (Mantel-Cox) test. Viral RNA in serum at 4 and 7 dpi and that in brain at 7 dpi were determined by qRT-PCR. The alanine aminotransferase (ALT) activity in serum at 7 dpi was detected using ALT activity assay kit (Sigma).

ZIKV Infection in Monkeys and Luminex Assay

Rhesus monkeys (*Macacamulatta*) were administered with EtOH or 25HC intravenously (i.v.) at 1.5 mg/kg of body weight 24 hr pre- or 4 hr post- intramuscular (i.m.) infection with 1×10^5 or 1×10^3 PFU of ZIKV GZ01 strain. They were subsequently treated with 25HC or EtOH daily for 7 days, and their body temperature and clinical signs were monitored daily. The blood and urine samples were collected from 0–7 dpi for viral load analysis by qRT-PCR. The serum collected at 0, 3, and 7 dpi were subjected to cytokine analysis with Monkey Cytokine Magnetic 29-Plex Panel (Thermo Fisher, LPC0005M) according to the manufacturer's instructions. The data were collected on Luminex200 and analyzed by Luminex xPONENT (Thermo Fisher).

ZIKV Infection in the Embryonic Mouse Brain

The ICR mice were pretreated with 25HC (50 mg/kg, i.p. injected) or vehicle (HβCD) 6 hr prior to viral infection. The right side of the lateral ventricle/LV of the E13.5 fetal brains were infected with 1 μL of ZIKV stock (6.5×10^5 PFU/mL) using glass micropipettes as described (Li et al., 2016a). Pregnant mice were treated with 25HC or vehicle (HβCD) 6 hr pre- and 6 hr post-ZIKV infection, followed by daily treatment for 5 days. For each pregnant dam, around ½ of the littermates were injected with ZIKV, and the others were injected with culture medium (mock) for proper controls.

Immunofluorescence Staining and Confocal Imaging and Quantification

For cryosections, tissues were fixed in 4% PFA then dehydrated in 30% sucrose and frozen in tissue freezing medium (TFM). Slices (thickness: 40 μm) were blocked at room temperature for 1 hr with 10% horse serum, 0.3% Triton X-100, and 5% BSA in PBS as described (Li et al., 2016a). The primary antibodies were applied overnight at the following concentrations: anti-phospho-histone3 (P-H3) (CST, 9701S, 1:1000), anti-activated-caspase3 (CST, 9664s, 1:500), anti-tbr1 (Abcam, ab31940, 1:500). Serumfrom a ZIKV-infected patient (1:100), a healthy non-ZIKV infected volunteer (1:100), or mice immunized with recombinant ZIKV FSS13025/2010 (GenBank: JN860885) envelope (E) protein was used (1:500). Nuclei were stained with DAPI (Thermo Fisher). Slices were imaged on an LSM 700 (Carl Zeiss) confocal microscope, and the images were analyzed with Imaris and ImageJ.

Accession Numbers

RNA-seq data have been deposited to Genome Sequence Archive of BIG Data Center, Beijing Institute of Genomics (BIG, CAS) under the accession number BIG: PRJCA000355.

Statistical Analysis

All data were analyzed using Prism software (GraphPad). Statistical evaluation was performed by Student's unpaired *t* test. Data are presented as mean ± SEM.

Supplementary Material

Refer to Web version on PubMed Central for supplementary material.

Acknowledgments

This work was supported by the CAMS Initiative for Innovative Medicine (No. 2016-I2M-1-005), National Science and Technology Major Project for "Significant New Drugs Innovation and Development" (2015ZX09102023), NSFC (China, 91542201, 81590765), NIH R01AI069120, AI056154, and AI078389 grants to G.C., PUMC Youth Fund (3332016125) and NSFC (31500145) to C.L., NSFC (31670883) to F.M., MOST (China, 2016YFD0500304) and the State Key Laboratory of Pathogen and Biosecurity (SKLPBS1601), the NSFC Excellent Young Scientist (81522025), the Innovative Research Group (81621005), and the Newton Advanced Fellowship from the UK Academy of Medical Sciences (NAF003/1003) and the NSFC of China (81661130162) to C.-F.Q., NSFC (31430037), Shanghai brain-intelligence project from STCSM (16JC1420500), Beijing brain project (Z161100002616004) and MOST (2014CB942801 and 2012YQ03026006) to Z.X., NIH R01 NS089817, CIRM DISC1-08819, and a research award from the UCLA Broad StemCell Research Center (BSCRC) to B.G.N. M.W. was supported by a training fellowship from the UCLABSCRC. We thank Natalie Quanquin (UCLA) and Lina Yuan (Suzhou Institute of Systems Medicine) for their help in editing the manuscript and RNA sequencing, respectively. We wish to thank Pei-Gang Wang (Capital Medical University, Beijing), Qi-Bin Leng (Institute Pasteur of Shanghai, CAS), Pei-Yong Shi (Novartis Institute for Infectious Diseases), and Guanghou Shui (Institute of Genetics and Developmental Biology, CAS), for providing us with critical reagents and helpful discussions.

References

Aye IL, Waddell BJ, Mark PJ, Keelan JA. Oxysterols exert proinflammatory effects in placental trophoblasts via TLR4-dependent, cholesterol-sensitive activation of NF-κB. Mol. Hum. Reprod. 2012; 18:341–353. [PubMed: 22238372]

Barrows NJ, Campos RK, Powell ST, Prasanth KR, Schott-Lerner G, Soto-Acosta R, Galarza-Muñoz G, McGrath EL, Urrabaz-Garza R, Gao J, et al. A Screen of FDA-Approved Drugs for Inhibitors of Zika Virus Infection. Cell Host Microbe. 2016; 20:259–270. [PubMed: 27476412]

Bauman DR, Bitmansour AD, McDonald JG, Thompson BM, Liang G, Russell DW. 25-Hydroxycholesterol secreted by macrophages in response to Toll-like receptor activation suppresses immunoglobulin A production. Proc. Natl. Acad. Sci. USA. 2009; 106:16764–16769. [PubMed: 19805370]

Bayer A, Lennemann NJ, Ouyang Y, Bramley JC, Morosky S, Marques ET Jr, Cherry S, Sadovsky Y, Coyne CB. Type III Interferons Produced by Human Placental Trophoblasts Confer Protection against Zika Virus Infection. Cell Host Microbe. 2016; 19:705–712. [PubMed: 27066743]

Bayless NL, Greenberg RS, Swigut T, Wysocka J, Blish CA. Zika Virus Infection Induces Cranial Neural Crest Cells to Produce Cytokines at Levels Detrimental for Neurogenesis. Cell Host Microbe. 2016; 20:423–428. [PubMed: 27693308]

Blanc M, Hsieh WY, Robertson KA, Kropp KA, Forster T, Shui G, Lacaze P, Watterson S, Griffiths SJ, Spann NJ, et al. The transcription factor STAT-1 couples macrophage synthesis of 25-hydroxycholesterol to the interferon antiviral response. Immunity. 2013; 38:106–118. [PubMed: 23273843]

Brasil P, Pereira JP Jr, Moreira ME, Ribeiro Nogueira RM, Damasceno L, Wakimoto M, Rabello RS, Valderramos SG, Halai UA, Salles TS, et al. Zika Virus Infection in Pregnant Women in Rio de Janeiro. N. Engl. J. Med. 2016; 375:2321–2334. [PubMed: 26943629]

Brown AJ, Jessup W. Oxysterols and atherosclerosis. Atherosclerosis. 1999; 142:1–28. [PubMed: 9920502]

Cao-Lormeau VM, Blake A, Mons S, Lastère S, Roche C, Vanhomwegen J, Dub T, Baudouin L, Teissier A, Larre P, et al. Guillain-Barré Syndrome outbreak associated with Zika virus infection in French Polynesia: a case-control study. Lancet. 2016; 387:1531–1539. [PubMed: 26948433]

Carteaux G, Maquart M, Bedet A, Contou D, Brugières P, Fourati S, Cleret de Langavant L, de Broucker T, Brun-Buisson C, Leparc-Goffart I, Mekontso Dessap A. Zika Virus Associated with Meningoencephalitis. N. Engl. J. Med. 2016; 374:1595–1596. [PubMed: 26958738]

Chen Y, Wang S, Yi Z, Tian H, Aliyari R, Li Y, Chen G, Liu P, Zhong J, Chen X, et al. Interferon-inducible cholesterol-25-hydroxylase inhibits hepatitis C virus replication via distinct mechanisms. Sci. Rep. 2014; 4:7242. [PubMed: 25467815]

Cugola FR, Fernandes IR, Russo FB, Freitas BC, Dias JL, Guimarães KP, Benazzato C, Almeida N, Pignatari GC, Romero S, et al. The Brazilian Zika virus strain causes birth defects in experimental models. Nature. 2016; 534:267–271. [PubMed: 27279226]

D'Ortenzio E, Matheron S, Yazdanpanah Y, de Lamballerie X, Hubert B, Piorkowski G, Maquart M, Descamps D, Damond F, Leparc-Goffart I. Evidence of Sexual Transmission of Zika Virus. N. Engl. J. Med. 2016; 374:2195–2198. [PubMed: 27074370]

Deng YQ, Zhang NN, Li CF, Tian M, Hao JN, Xie XP, Shi PY, Qin CF. Adenosine Analog NITD008 Is a Potent Inhibitor of Zika Virus. Open Forum Infect. Dis. 2016; 3:ofw175. [PubMed: 27747251]

Dick GW, Kitchen SF, Haddow AJ. Zika virus. I. Isolations and serological specificity. Trans. R. Soc. Trop. Med. Hyg. 1952; 46:509–520. [PubMed: 12995440]

Driggers RW, Ho CY, Korhonen EM, Kuivanen S, Jääskeläinen AJ, Smura T, Rosenberg A, Hill DA, DeBiasi RL, Vezina G, et al. Zika Virus Infection with Prolonged Maternal Viremia and Fetal Brain Abnormalities. N. Engl. J. Med. 2016; 374:2142–2151. [PubMed: 27028667]

Dudley DM, Aliota MT, Mohr EL, Weiler AM, Lehrer-Brey G, Weisgrau KL, Mohns MS, Breitbach ME, Rasheed MN, Newman CM, et al. A rhesus macaque model of Asian-lineage Zika virus infection. Nat. Commun. 2016; 7:12204. [PubMed: 27352279]

Garcez PP, Loiola EC, Madeiro da Costa R, Higa LM, Trindade P, Delvecchio R, Nascimento JM, Brindeiro R, Tanuri A, Rehen SK. Zika virus impairs growth in human neurospheres and brain organoids. Science. 2016; 352:816–818. [PubMed: 27064148]

Holmes RS, Vandeberg JL, Cox LA. Genomics and proteomics of vertebrate cholesterol ester lipase (LIPA) and cholesterol 25-hydroxylase (CH25H). 3 Biotech. 2011; 1:99–109.

Iwasaki A, Pillai PS. Innate immunity to influenza virus infection. Nat. Rev. Immunol. 2014; 14:315–328. [PubMed: 24762827]

Janowski BA, Grogan MJ, Jones SA, Wisely GB, Kliewer SA, Corey EJ, Mangelsdorf DJ. Structural requirements of ligands for the oxysterol liver X receptors LXRalpha and LXRbeta. Proc. Natl. Acad. Sci. USA. 1999; 96:266–271. [PubMed: 9874807]

Larkin JC, Sears SB, Sadovsky Y. The influence of ligand-activated LXR on primary human trophoblasts. Placenta. 2014; 35:919–924. [PubMed: 25255963]

Larocca RA, Abbink P, Peron JP, Zanotto PM, Iampietro MJ, Badamchi-Zadeh A, Boyd M, Ng'ang'a D, Kirilova M, Nityanandam R, et al. Vaccine protection against Zika virus from Brazil. Nature. 2016; 536:474–478. [PubMed: 27355570]

Lazear HM, Govero J, Smith AM, Platt DJ, Fernandez E, Miner JJ, Diamond MS. A Mouse Model of Zika Virus Pathogenesis. Cell Host Microbe. 2016; 19:720–730. [PubMed: 27066744]

Li C, Xu D, Ye Q, Hong S, Jiang Y, Liu X, Zhang N, Shi L, Qin CF, Xu Z. Zika Virus Disrupts Neural Progenitor Development and Leads to Microcephaly in Mice. Cell Stem Cell. 2016a; 19:120–126. [PubMed: 27179424]

Li XF, Dong HL, Huang XY, Qiu YF, Wang HJ, Deng YQ, Zhang NN, Ye Q, Zhao H, Liu ZY, et al. Characterization of a 2016 Clinical Isolate of Zika Virus in Non-human Primates. EbioMedicine. 2016b; 12:170–177. [PubMed: 27693104]

Liu SY, Sanchez DJ, Aliyari R, Lu S, Cheng G. Systematic identification of type I and type II interferon-induced antiviral factors. Proc. Natl. Acad. Sci. USA. 2012; 109:4239–4244. [PubMed: 22371602]

Liu SY, Aliyari R, Chikere K, Li G, Marsden MD, Smith JK, Pernet O, Guo H, Nusbaum R, Zack JA, et al. Interferon-inducible cholesterol- 25-hydroxylase broadly inhibits viral entry by production of 25-hydroxycholesterol. Immunity. 2013; 38:92–105. [PubMed: 23273844]

Ma W, Li S, Ma S, Jia L, Zhang F, Zhang Y, Zhang J, Wong G, Zhang S, Lu X, et al. Zika virus causes testis damage and leads to male infertility in mice. Cell. 2016; 167:1511–1524. [PubMed: 27884405]

Miner JJ, Cao B, Govero J, Smith AM, Fernandez E, Cabrera OH, Garber C, Noll M, Klein RS, Noguchi KK, et al. Zika Virus Infection during Pregnancy in Mice Causes Placental Damage and Fetal Demise. Cell. 2016; 165:1081–1091. [PubMed: 27180225]

Moog C, Aubertin AM, Kirn A, Luu B. Oxysterols, but not cholesterol, inhibit human immunodeficiency virus replication in vitro. Antivir. Chem. Chemother. 1998; 9:491–496. [PubMed: 9865387]

Musso D, Gubler DJ. Zika Virus. Clin. Microbiol. Rev. 2016; 29:487–524. [PubMed: 27029595]

Osuna CE, Lim SY, Deleage C, Griffin BD, Stein D, Schroeder LT, Omange R, Best K, Luo M, Hraber PT, et al. Zika viral dynamics and shedding in rhesus and cynomolgus macaques. Nat. Med. 2016; 22:1448–1455. [PubMed: 27694931]

Park K, Scott AL. Cholesterol 25-hydroxylase production by dendritic cells and macrophages is regulated by type I interferons. J. Leukoc. Biol. 2010; 88:1081–1087. [PubMed: 20699362]

Qian X, Nguyen HN, Song MM, Hadiono C, Ogden SC, Hammack C, Yao B, Hamersky GR, Jacob F, Zhong C, et al. Brain-Region-Specific Organoids Using Mini-bioreactors for Modeling ZIKV Exposure. Cell. 2016; 165:1238–1254. [PubMed: 27118425]

Rasmussen SA, Jamieson DJ, Honein MA, Petersen LR. Zika Virus and Birth Defects–Reviewing the Evidence for Causality. N. Engl. J. Med. 2016; 374:1981–1987. [PubMed: 27074377]

Sadler AJ, Williams BR. Interferon-inducible antiviral effectors. Nat. Rev. Immunol. 2008; 8:559–568. [PubMed: 18575461]

Savidis G, Perreira JM, Portmann JM, Meraner P, Guo Z, Green S, Brass AL. The IFITMs Inhibit Zika Virus Replication. Cell Rep. 2016; 15:2323–2330. [PubMed: 27268505]

Shibata N, Carlin AF, Spann NJ, Saijo K, Morello CS, McDonald JG, Romanoski CE, Maurya MR, Kaikkonen MU, Lam MT, et al. 25-Hydroxycholesterol activates the integrated stress response to reprogram transcription and translation in macrophages. J. Biol. Chem. 2013; 288:35812–35823. [PubMed: 24189069]

Talarico LB, Pujol CA, Zibetti RG, Faría PC, Noseda MD, Duarte ME, Damonte EB. The antiviral activity of sulfated polysaccharides against dengue virus is dependent on virus serotype and host cell. Antiviral Res. 2005; 66:103–110. [PubMed: 15911027]

Tang H, Hammack C, Ogden SC, Wen Z, Qian X, Li Y, Yao B, Shin J, Zhang F, Lee EM, et al. Zika Virus Infects Human Cortical Neural Progenitors and Attenuates Their Growth. Cell Stem Cell. 2016; 18:587–590. [PubMed: 26952870]

Wang F, Xia W, Liu F, Li J, Wang G, Gu J. Interferon regulator factor 1/retinoic inducible gene I (IRF1/RIG-I) axis mediates 25-hydroxycholesterol-induced interleukin-8 production in atherosclerosis. Cardiovasc. Res. 2012; 93:190–199. [PubMed: 21979142]

Woollett LA. Fetal Lipid Metabolism. Front. Biosci. 2001; 6:D536–D545. [PubMed: 11229883]

Xu M, Lee EM, Wen Z, Cheng Y, Huang WK, Qian X, Tcw J, Kouznetsova J, Ogden SC, Hammack C, et al. Identification of small-molecule inhibitors of Zika virus infection and induced neural cell death via a drug repurposing screen. Nat. Med. 2016; 22:1101–1107. [PubMed: 27571349]

Yin Z, Chen YL, Schul W, Wang QY, Gu F, Duraiswamy J, Kondreddi RR, Niyomrattanakit P, Lakshminarayana SB, Goh A, et al. An adenosine nucleoside inhibitor of dengue virus. Proc. Natl. Acad. Sci. USA. 2009; 106:20435–20439. [PubMed: 19918064]

Zaitseva E, Yang ST, Melikov K, Pourmal S, Chernomordik LV. Dengue virus ensures its fusion in late endosomes using compartment- specific lipids. PLoS Pathog. 2010; 6:e1001131. [PubMed: 20949067]

Zhang NN, Tian M, Deng YQ, Hao JN, Wang HJ, Huang XY, Li XF, Wang YG, Zhao LZ, Zhang FC, Qin CF. Characterization of the contemporary Zika virus in immunocompetent mice. Hum. Vaccin. Immunother. 2016; 12:3107–3109. [PubMed: 27603093]

Zmurko J, Marques RE, Schols D, Verbeken E, Kaptein SJ, Neyts J. The Viral Polymerase Inhibitor 7-Deaza-2′-C-Methyladenosine Is a Potent Inhibitor of In Vitro Zika Virus Replication and Delays Disease Progression in a Robust Mouse Infection Model. PLoS Negl. Trop. Dis. 2016; 10:e0004695. [PubMed: 27163257]

Highlights

- CH25H and its enzymatic product, 25HC, inhibit ZIKV entry in vitro
- 25HC attenuates ZIKV-associated viremia and disease in mice and non-human primates
- 25HC prevents ZIKV infection in human cortical organoids
- 25HC protects fetal mice from microcephaly caused by ZIKV infection

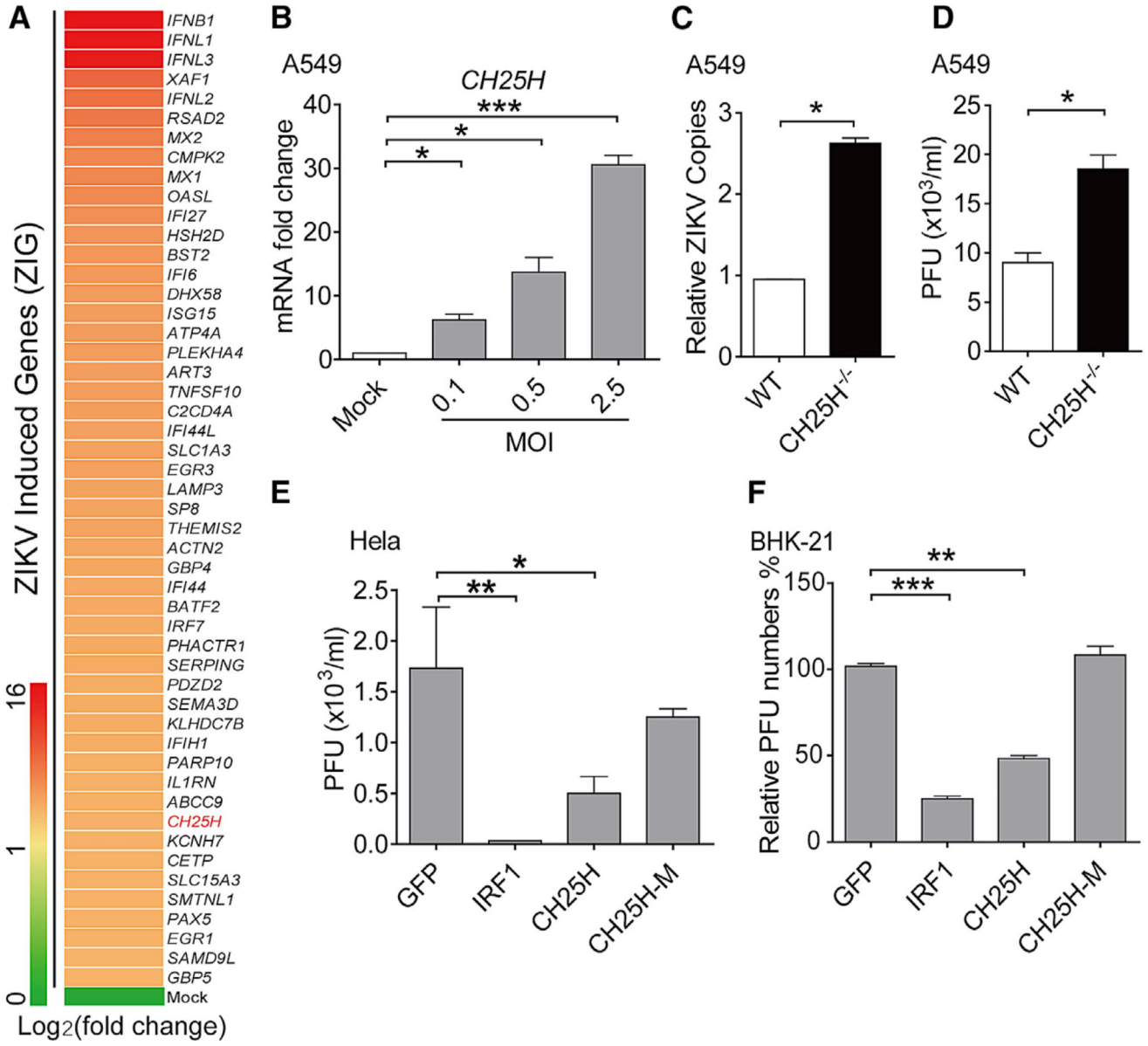

Figure 1. ZIKV-Triggered Induction of CH25H Plays an Important Role in Host Anti-ZIKV Immunity

(A) A549 cells were infected with ZIKV (GZ01/2016 strain, MOI 5) for 24 hr, RNA-seq was performed, and the top 50 genes upregulated by ZIKV infection in A549 cells were shown.

(B) A549 cells were infected with indicated MOI of ZIKV (GZ01/2016 strain) for 24 hr, *CH25H* mRNA expression was measured by qRT-PCR.

(C and D) WT and *CH25H*$^{-/-}$ A549 cells were infected with ZIKV (GZ01/2016 strain, MOI 0.1) for 48 hr, ZIKV in cell lysates, and the supernatant was measured by qRT-PCR (C) and plaque assay (D), respectively.

(E) HeLa cells were transfected with plasmids expressing GFP, IRF1, CH25H, or CH25H-M (hydroxylase activity-dead mutant) for 24 hr, followed by infecting cells with ZIKV

(GZ01/2016 strain) for 48 hr at MOI of 0.1. The titer of ZIKV in the supernatant was quantified by plaque assay.

(F) BHK-21 cells were treated with conditioned media from HeLa cells expressing the indicated genes for 12 hr and infected with ZIKV (GZ01/2016 strain, 200PFU). Then, the BHK-21 cells were subjected to plaque assay.

Data of (B)–(F) are shown as mean ± SEM from three independent experiments. *$p \leq 0.05$, **$p \leq 0.01$, ***$p \leq 0.001$, unpaired Student's *t* test. See also Figure S1–S3.

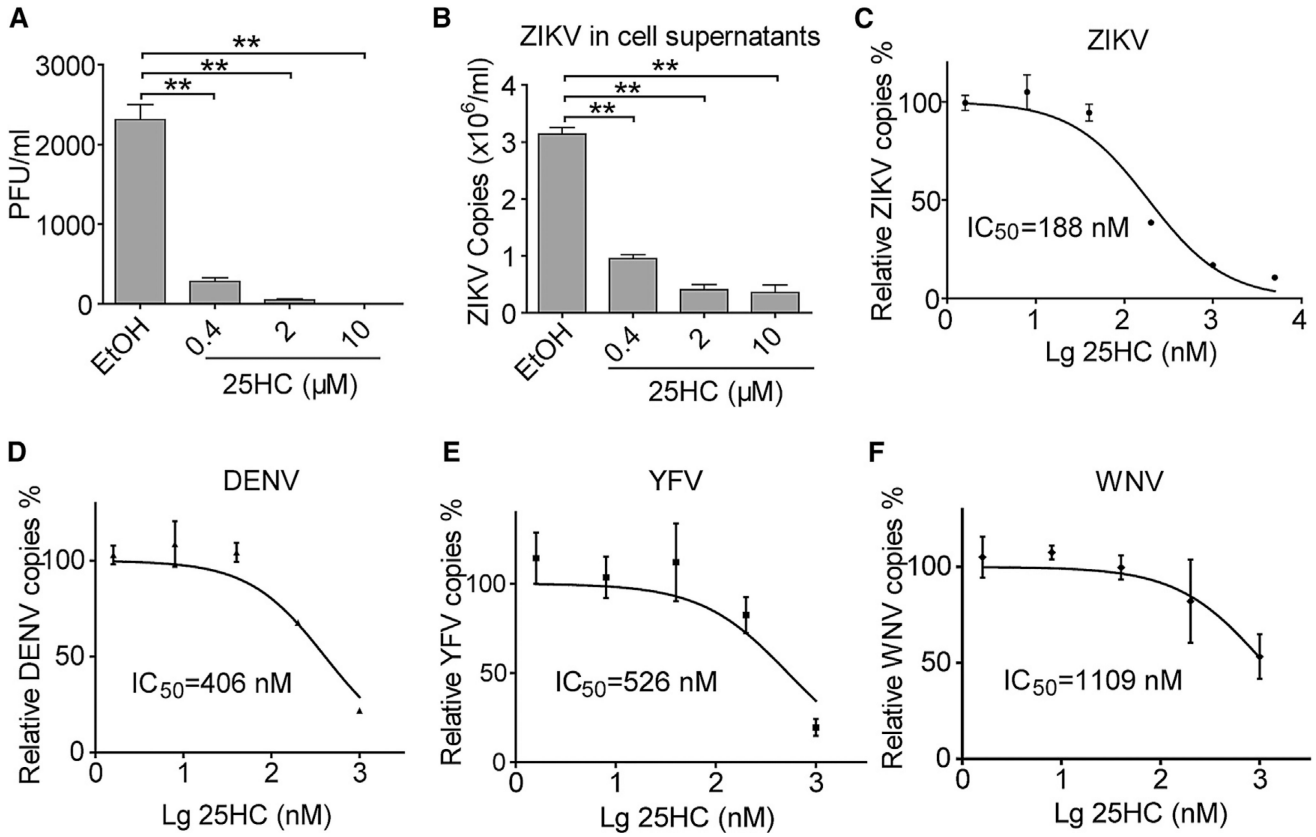

Figure 2. 25HC Broadly Inhibits Flaviviruses Infection

(A and B) Vero cells were pretreated with EtOH or indicated dose of 25HC for 8 hr, followed by ZIKV infection (GZ01/2016 strain, MOI 0.1). The titer of ZIKV in the supernatant was quantified by (A) plaque assay and (B) qRT-PCR.

(C–F) Vero cells were pretreated with indicated amount of 25HC for 8 hr and then infected with (C) ZIKV GZ01/2016 strain, (D) DENV, (E) YFV, and (F) WNV at MOI 0.1. Viral RNA copies in cell lysates were quantified by qRT-PCR. IC_{50} of 25HC to ZIKV, DENV, YFV, and WNV were calculated and indicated. All data are shown as mean ± SEM from three independent experiments. **p ≤ 0.01, unpaired Student's *t* test. See also Figure S4.

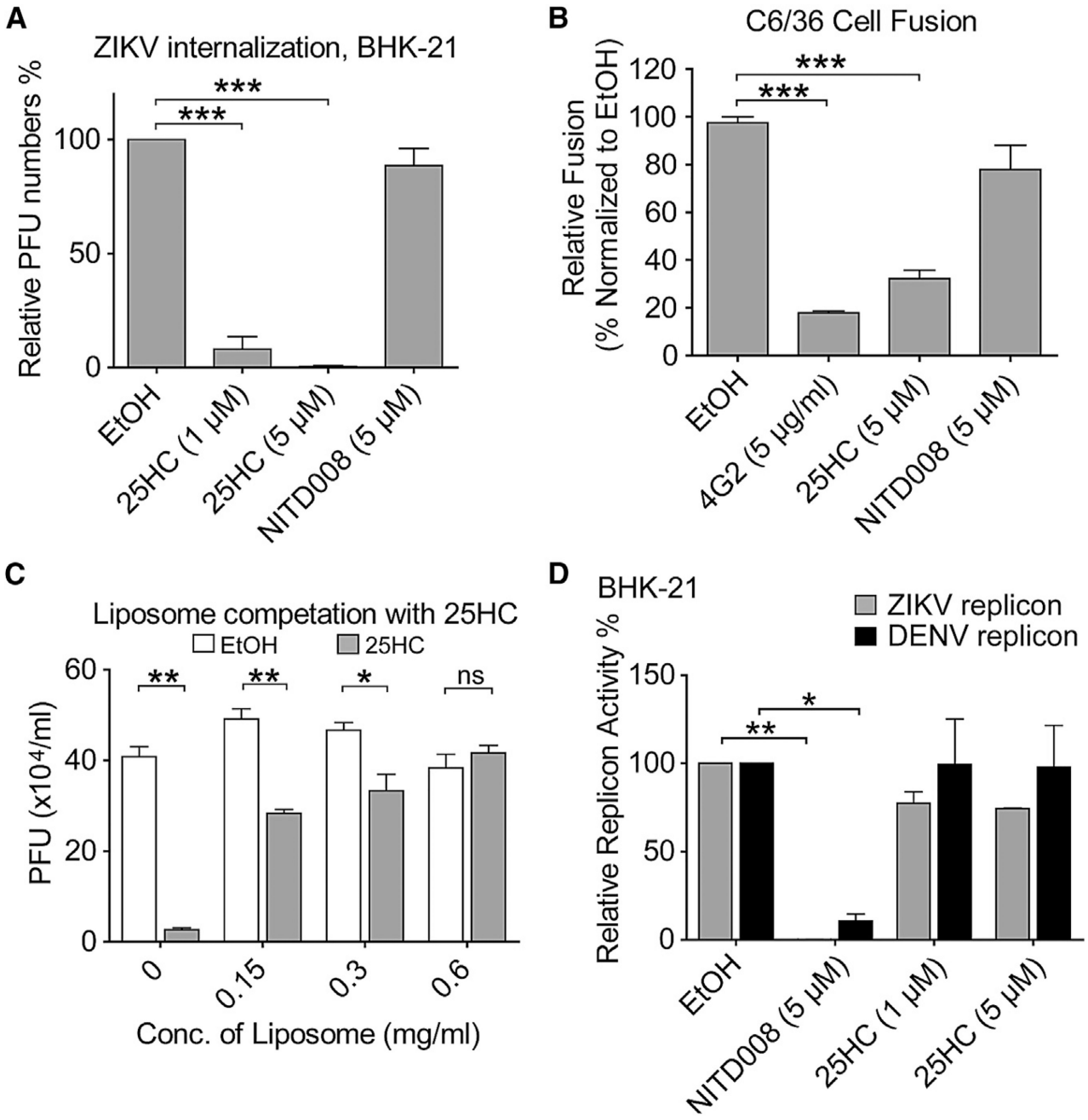

Figure 3. 25HC Suppressed ZIKV Infection by Blocking Viral Entry

(A) BHK-21 cells were treated with EtOH, 1 and 5 μM 25HC, and NITD008 for 12 hr, followed by infecting cells with ZIKV (GZ01/2016 strain, 200 PFU/well) at 4°C for 1 hr. Cells were washed with cold PBS and incubated at 37°C for 1 hr. The titer of internalized virus was measured with plaque assay.

(B) C6/36 cells were infected with DENV (MOI 0.2) for 4 days and treated with 25HC for another 8 hr. Syncythia formation was stimulated with medium (pH 5.8) for 2 hr and then replaced with fresh regular medium. 24 hr post stimulation, C6/36 cells were stained with Giemsa. 4G2 and NITD008 were used as positive and negative controls, respectively.

Syncythias were defined as the cells containing four or more nuclei. The number of syncythias in samples with EtOH was set to 100%.

(C) A549 cells were pretreated with indicated concentration of Liposome, and 25HC or EtOH, for 8 hr. Cells were infected with ZIKV (GZ01/2016 strain, MOI 0.3) in 37°C, followed by plaque assay at 48 hpi.

(D) BHK-21 cells were transfected with RNA from ZIKV/DENV replicon. 6 hr post transfection, 25HC was added into cells, and subsequently, renilla luciferase activity in cell lysates was determined at 48 hr post transfection. NITD008 was used as positive control. All data are shown as mean ± SEM from three independent experiments, *$p \leq 0.05$, **$p \leq 0.01$, ***$p \leq 0.001$, unpaired Student's *t* test. See also Figure S5.

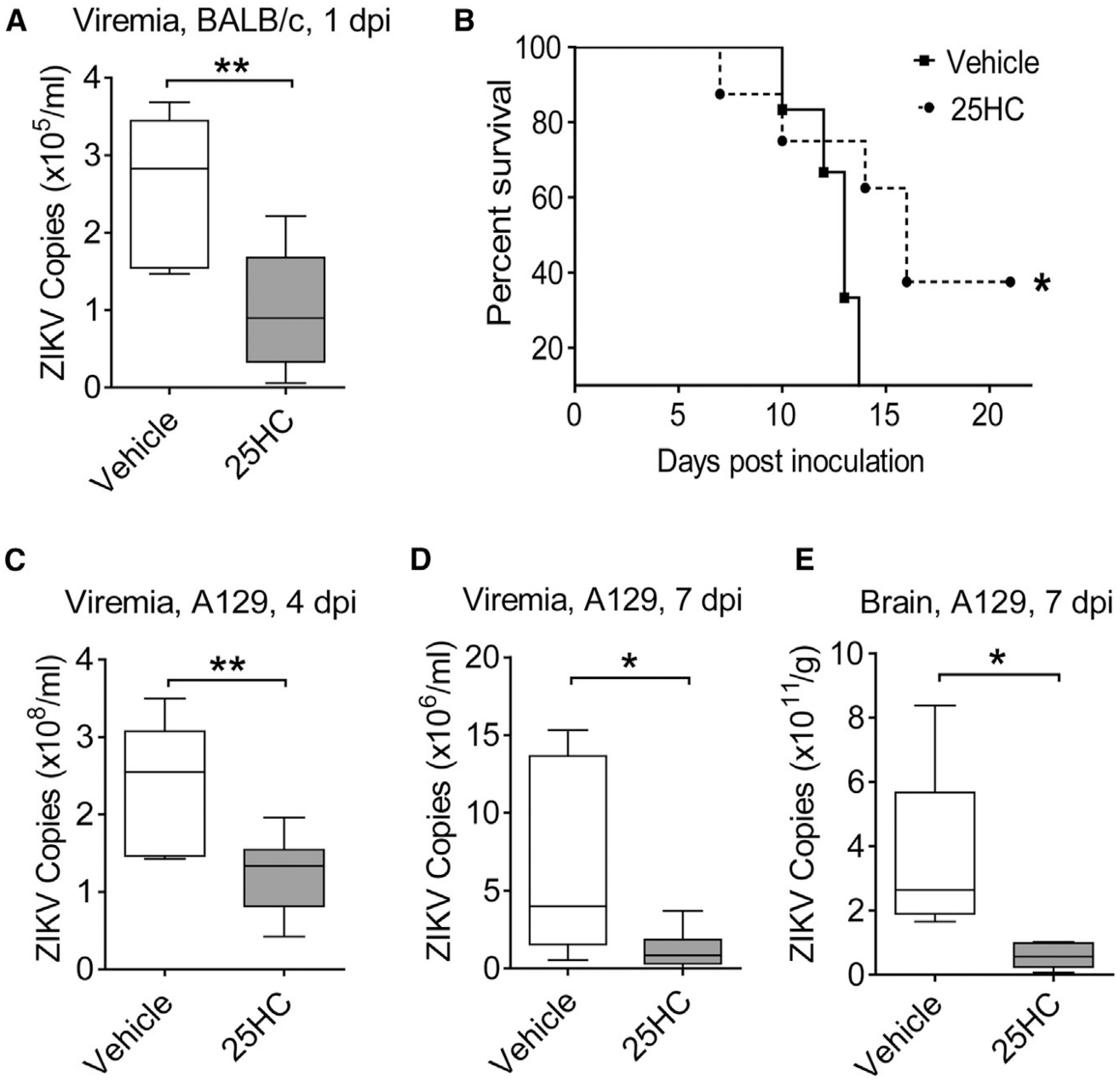

Figure 4. 25HC Reduces ZIKV Viremia and Improves Survival in Mice

(A) 3- to 4 week-old female BALB/c mice were injected i.p. with 25HC (50 mg/kg) or vehicle HβCD for 12 hr and subjected to ZIKV infection i.p. (1×10^5 PFU GZ01/2016 strain). The viral copy number in serum was quantified by qRT-PCR at 1 dpi. Vehicle: n = 6; 25HC: n = 9.

(B–E) 3- to 4-week-old female A129 mice were pretreated with 25HC or vehicle as described in (A) and 12 hr later were infected i.p. with 2×10^5 PFU (B) or 2×10^3 PFU (C–E) ZIKV (GZ01/2016 strain). 25HC or vehicle were administrated daily for seven days. (B) The rate of mice survival until 21 dpi and (C) the level of ZIKV RNA in serum at 4 dpi (D) and 7 dpi (E) and in the brain were measured by qRT-PCR.

Log-Rank (Mantel-Cox) test were used in (B), vehicle: n = 6; 25HC: n = 8 *p ≤ 0.05. Median value of (A, C–E) has been shown, vehicle: n = 7; 25HC: n = 8 (C and D); vehicle/25HC: n = 5 (E). *p ≤ 0.05, **p ≤ 0.01, unpaired Student's *t* test.

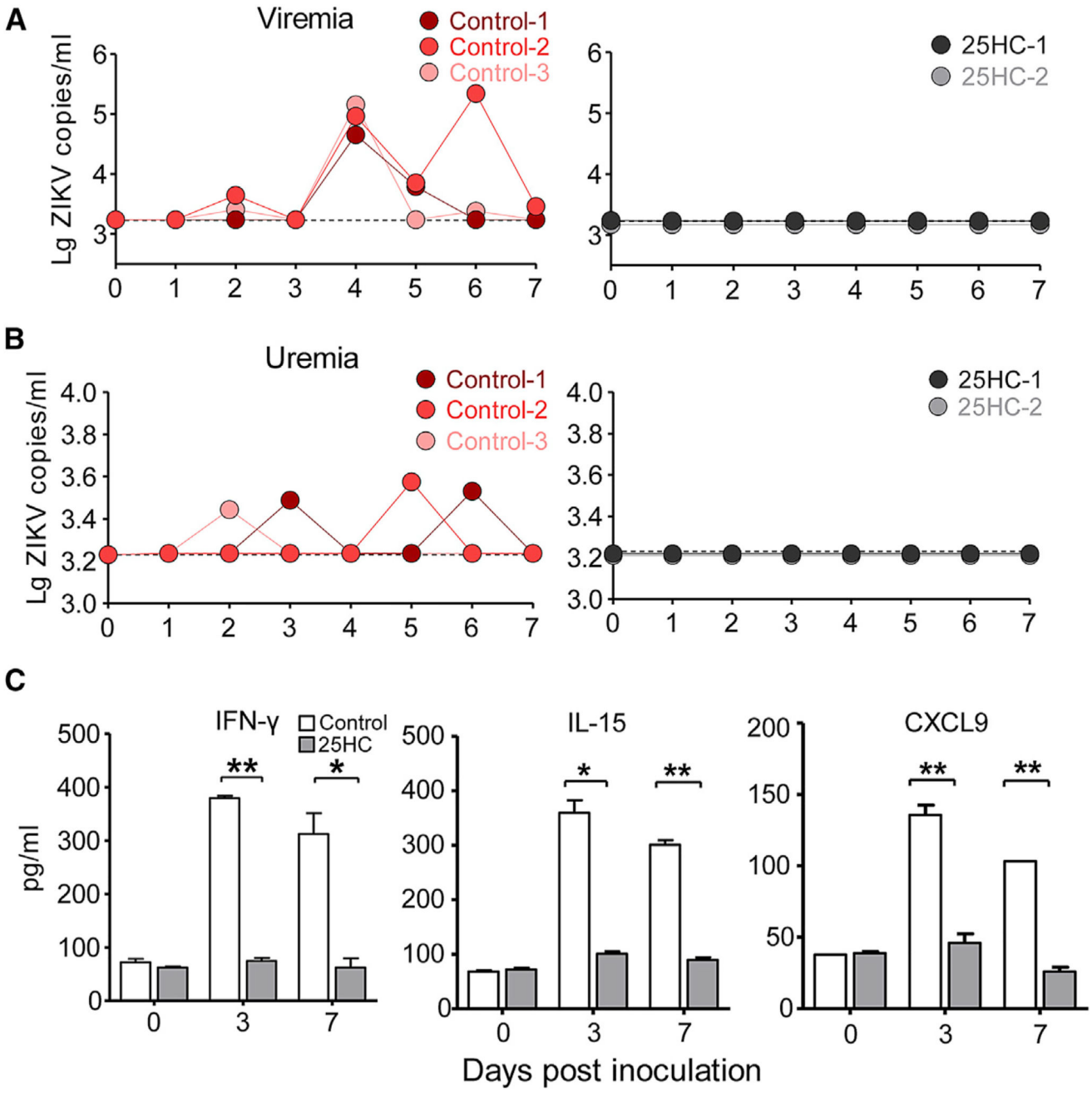

Figure 5. 25HC Protects Rhesus Monkeys from ZIKV Infection

(A and B) Rhesus monkeys were injected i.v. with 25HC (1.5 mg/kg) (n = 2) or the vehicle control EtOH (n = 3), followed by infection with 1×10^3 PFU of ZIKV (GZ01/2016 strain) *i.m.* Animals were treated with 25HC or EtOH daily for 7 days. Viral copy numbers in (A) serum and (B) urine of control monkeys or 25HC-pretreated were measured by qRT-PCR. (C) The level of IFN-γ, IL-15, and CXCL9 in the serum of infected animals was measured at 0, 3, and 7 dpi by Luminex assay. Data of (C) are shown as mean ± SD from three experimental replicates, *p ≤ 0.05, **p ≤ 0.01, unpaired Student's *t* test.

See also Figure S6.

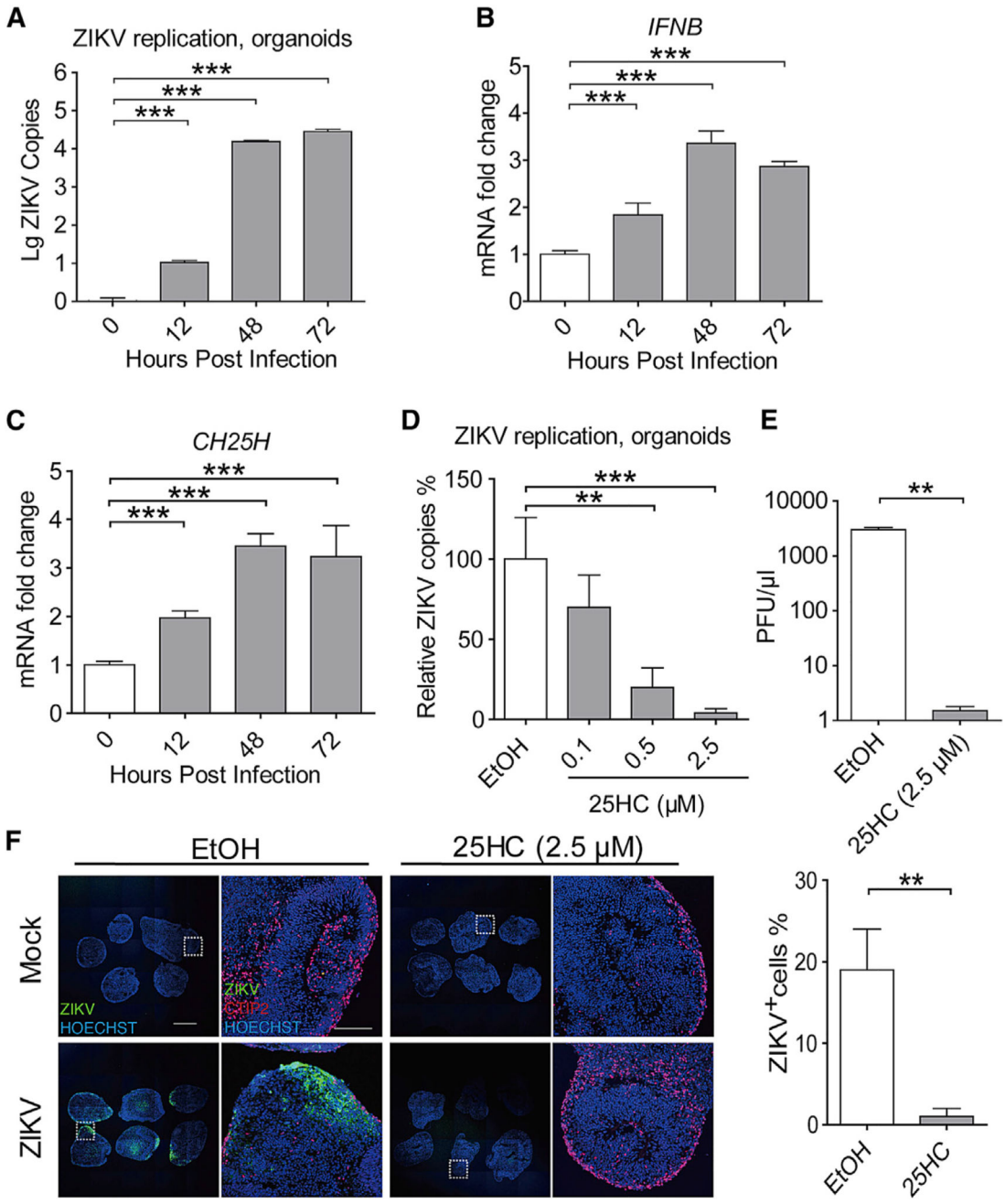

Figure 6. 25HC Inhibits ZIKV Infection in Human Cortical Organoids

Human cortical organoids were differentiated from hES. On day 20, these organoids were inoculated with ZIKV (PRVABC59/2015 strain, MOI 1).

(A–C) Organoids were inoculated with ZIKV for indicated time, and expression of ZIKV genomic RNA (A), *IFNB* (B), and *CH25H* (C) was quantified by qRT-PCR.

(D–F) Human cortical organoids were pretreated with indicated dose of 25HC or EtOH for 15 hr and then infected with ZIKV for 48 hr. ZIKV genomic RNA and titer were quantified by (D) qRT-PCR or (E) plaque assay. (F) Left: ZIKV E protein in these organoids was stained by immunofluorescence assay. Right: $ZIKV^{+}$ cells were also quantified. Green:

ZIKV E protein; blue: HOECHST; red: CTIP2. Scale bars; left, 500 μm; right, 100 μm. Data of (A–E) are shown as mean ± SEM from three independent experiments, **p ≤ 0.01, ***p ≤ 0.001, unpaired Student's *t* test. Data of (F) are representative of three independent experiments.

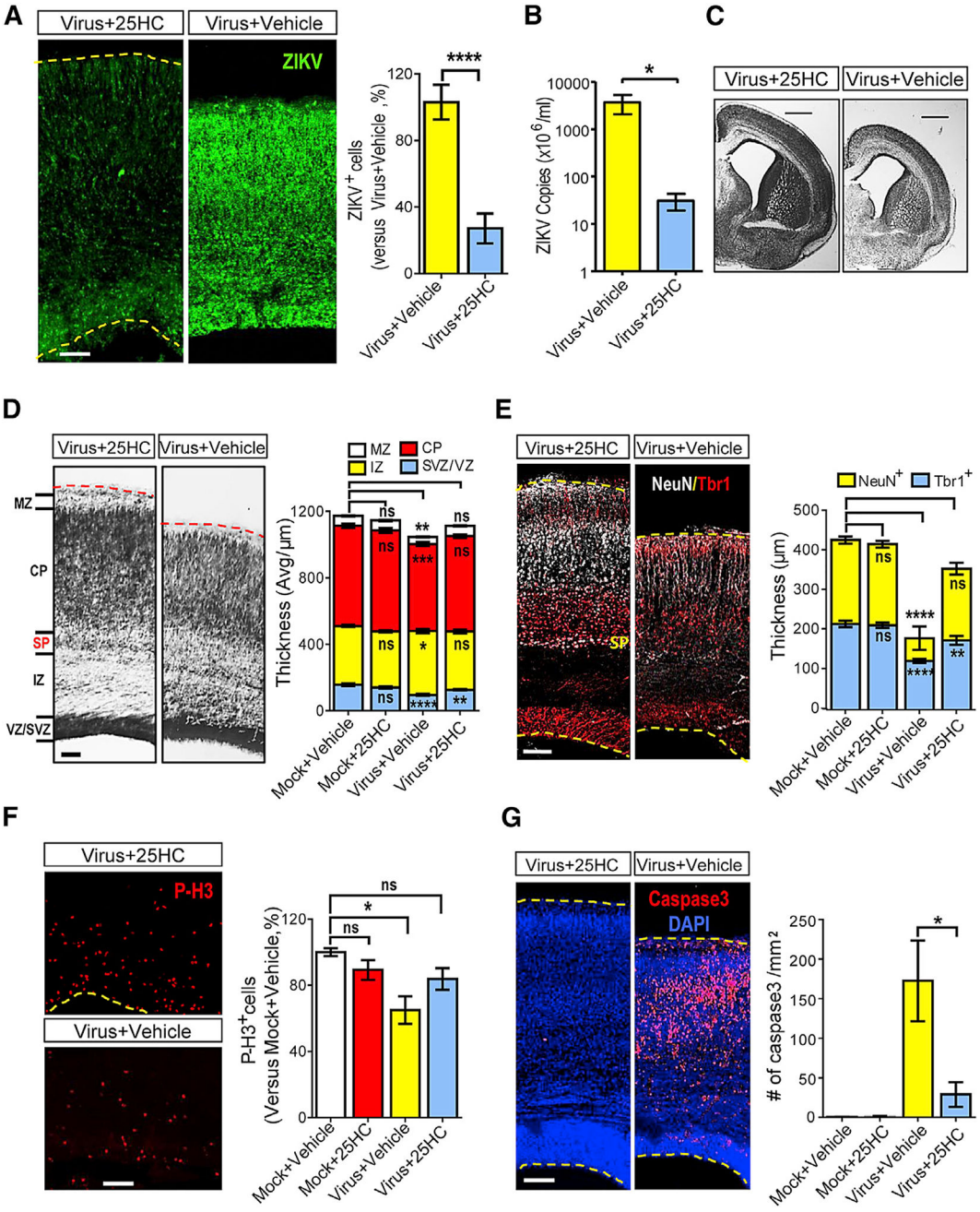

Figure 7. 25HC Protects the Embryonic Brains from ZIKV-Induced Microcephaly

Embryonic brains were injected with ZIKV (SZ01/2016, 650 PFU/brain) or medium at E13.5 and inspected at E18.5 with or without treatment with 25HC (50 mg/kg, i.p.)

(A) Coronal sections were stained with ZIKV antiserum (green, left panel) and ZIKV$^+$ cells were quantified (right panel). Virus+25HC: n = 9; Virus+Vehicle: n = 10.

(B) ZIKV genomic RNA copies were measured by qRT-PCR, n = 3.

(C) Similar positions of coronal sections were Nissl-stained, scale bars, 1mm.

(D) Nissl staining was shown for the ZIKV-infected cortices with or without 25HC treatment (left). The thickness of different layers was measured (right), n = 20 for each group. MZ:

marginal zone; CP: cortical plate; SP: sub-plate; IZ: intermediate zone; SVZ: sub-ventricle zone; VZ: ventricle zone.

(E) Cortices were stained for Tbr1 (early born post-mitotic neuron marker, red) and NeuN (general post-mitotic neuron marker, white) (left). The thickness of the layers with individual markers was stained. Mock+Vehicle: n = 14 ($Tbr1^+$), 8 ($NeuN^+$); Mock+25HC: n = 15 ($Tbr1^+$), 12 ($NeuN^+$); Virus+Vehicle: n = 15 ($Tbr1^+$), 11 ($NeuN^+$); Virus+25HC: n = 12 ($Tbr1^+$), 11 ($NeuN^+$).

(F) Cortices were stained with Phospho-Histone H3 (red, left). Relative $P\text{-}H3^+$ cells in the cortex were quantified (right).

(G) Cortices were stained with the activated form of caspase3 (red) and DAPI (blue) (left), $caspase3^+$ cells were quantified (right).

Data of (A), (B), and (D)–(G) are shown as means ± SEM from three independent experiments, *$p \leq 0.05$, **$p \leq 0.01$, ***$p \leq 0.001$, ****$p \leq 0.0001$, unpaired Student's *t* test. Scale bars for (A) and (D)–(G): 100 μm.